Electrochemical Synthesis and Structural and Physical Characterization of One- and Two-Electron-Reduced Forms of $[SMo_{12}O_{40}]^{2-}$

Truc Vu,[†] Alan M. Bond,*[,†] David C. R. Hockless,[‡] Boujemaa Moubaraki,[†] Keith S. Murray,[†] Georgii Lazarev,[†] and Anthony G. Wedd[§]

Department of Chemistry, PO Box 23, Monash University, Victoria 3800, Australia, Research School of Chemistry, The Australian National University, Canberra, ACT 0200, Australia, and School of Chemistry, University of Melbourne, Parkville, Victoria 3052, Australia

Received November 9, 1999

Isolation of a soluble $[NHex_4]^+$ salt has allowed a detailed electrochemical study of the anion α-$[SMo_{12}O_{40}]^{2-}$ to be undertaken. Four reversible one-electron-reduction processes are observed in CH_2Cl_2 solution. Controlled potential electrolysis led to isolation of tetraalkylammonium salts of the one-electron-reduced anion α-$[SMo_{12}O_{40}]^{3-}$ and the two-electron-reduced anion α-$[SMo_{12}O_{40}]^{4-}$. $[SMo_{12}O_{40}]^{3-}$ is stable to disproportionation in dry solvents ($K_{dis} = 10^{-7.4}$). EPR and magnetic susceptibility data indicate that $[SMo_{12}O_{40}]^{3-}$ is a simple paramagnet ($S = {}^1/_2$) while $[SMo_{12}O_{40}]^{4-}$ is paramagnetic with the μ_{eff} values decreasing at low temperatures. Solutions of the two-electron-reduced species are EPR silent, but microcrystalline powders show very weak signals. The crystal structure of α-$[NBu_4]_3[SMo_{12}O_{40}]$ has been determined (triclinic $P\bar{1}$; $a = 13.840(3)$ Å; $b = 15.587(4)$ Å; $c = 19.370(3)$ Å; $\alpha = 94.82(2)^o$; $\beta = 93.10(1)^o$; $\gamma = 91.05(2)^o$; $Z = 2$). There is disorder around the C_2 axis of the central SO_4^{2-} tetrahedron. In the presence of aqueous $HClO_4$ (0.045 M) in thf/H_2O or MeCN/H_2O (98/2 v/v), $[SMo_{12}O_{40}]^{2-}$ exhibits five two-electron-reduction processes. Under these conditions, $[SMo_{12}O_{40}]^{3-}$ protonates and disproportionates into $[SMo_{12}O_{40}]^{2-}$ and the ($2e^-$, $2H^+$)-reduced anion $[H_2SMo_{12}O_{40}]^{2-}$.

Introduction[1]

Polyoxometalates continue to be studied intensively because of their photochemical, catalytic, and redox properties as well as their applications in commercially important processes or technologies.[2] An important electrochemical aspect is their well-developed redox and photochemical properties, coupled to resistance to oxidative degradation. For example, the presence of heteroatoms S^{VI} in the Dawson anion $[S_2Mo_{18}O_{62}]^{4-}$ imposes a relatively low anionic charge and consequent positive reduction potentials.[3,4] A rich redox chemistry follows, including an ability to accept up to 26 electrons,[5] to form air-stable salts reduced by 1, 2, or 4 electrons,[6,7] and to act as a powerful photooxidant.[8,9] The related but simpler Keggin anion $[SMo_{12}O_{40}]^{2-}$ (I) is an obvious target for comparative study of the properties of Dawson and Keggin structures which are both important in catalysis, in molecular materials, and in supramolecular assemblies.[10] However, while the synthesis and structural characterization of $[SMo_{12}O_{40}]^{2-}$ as tetraalkylammonium salts have been reported, poor solubility has restricted a fuller characterization of reduced forms.[11−15] The present work reports that α-$[NHex_4]_2[SMo_{12}O_{40}]$ is soluble in a range of organic solvents, which has permitted for a more detailed examination of the redox properties to be undertaken. In particular, electrochemical studies have enabled a detailed characterization of extended series of electron transfer steps, the role of proton addition reactions to be established with highly basic reduced forms and isolation in substance, and characterization of salts of the one- and two-electron-reduced anions $[SMo_{12}O_{40}]^{3-}$ and $[SMo_{12}O_{40}]^{4-}$.

Experimental Section

Reagents: $Na_2MoO_4 \cdot 2H_2O$ (BDH, AR grade), $HClO_4$ (BDH, Analar 60% aqueous solution), NR_4ClO_4 (R = Bu, Hex; GFS, electrometric

* E-mail: Alan.Bond@sci.monash.edu.au. Fax: +61 3 9905 9129.
[†] Monash University.
[‡] The Australian National University.
[§] University of Melbourne.

(1) Abbreviations: Bu, *n*-C_4H_9; *d*, diameter; CV, cyclic voltammetry; *D*, diffusion coefficient; ΔE_p, peak-to-peak separation; *E*, potential; $E_{1/2}$, half-wave potential; $E^r_{1/2}$, reversible half-wave potential; ES-MS, electrospray mass spectrometry; *F*, Faraday's constant; Fc, Fe(η^5-C_5H_5)$_2$; Hex, *n*-C_6H_{13}; *K*, equilibrium constant; *n*, number of electrons transferred per mole; OTTLE, optically transparent thin layer electrode; *T*, temperature; thf, tetrahydrofuran; *ν*, scan rate.

(2) (a) Wienstock, I. A. *Chem. Rev.* **1998**, *98*, 113−170. (b) Kozhenvnikov, I. V. *Chem. Rev.* **1998**, *98*, 171−198. (c) Mizuno, N.; Misono, M. *Chem. Rev.* **1998**, *98*, 199−217. (d) Sadakane, M.; Steckhan, E. *Chem. Rev.* **1998**, *98*, 219−237. (e) Yamase, T. *Chem. Rev.* **1998**, *98*, 307−325. (f) Rhule, J. T.; Hill, C. L.; Judd, D. A.; Schinazi, R. F. *Chem. Rev.* **1998**, *98*, 327−357.
(3) Baker, L. C. W.; Glick, D. C. *Chem. Rev.* **1998**, *98*, 3−49.
(4) Himeno, S.; Hori, T.; Saito, A. *Bull. Chem. Soc. Jpn.* **1989**, *62*, 2184−2188.
(5) Way, D. M.; Bond, A. M.; Wedd, A. G. *Inorg. Chem.*, **1997**, *36*, 2826−2833.
(6) Way, D. M.; Cooper, J. B.; Sadek, M.; Vu, T.; Mahon, P. J.; Bond, A. M.; Brownlee, R. T. C.; Wedd, A. G. *Inorg. Chem.* **1997**, *36*, 4227−4233.
(7) Neier, R.; Trojanowski, C.; Mattes, R. *J. Chem. Soc., Dalton Trans.* **1995**, 2521−2528.
(8) Bond, A. M.; Way, D. M.; Wedd, A. G.; Compton, R. G.; Booth, J.; Eklund, J. C. *Inorg. Chem.* **1995**, *34*, 3378−3384.
(9) Bond, A. M.; Eklund, J. C.; Tedesco, V.; Vu, T.; Wedd, A. G. *Inorg. Chem.* **1998**, *37*, 2366−2372.
(10) Coronado, E.; Gómez-García, C. J. *Chem. Rev.* **1998**, 98, 273−296.
(11) Cartié, B. *J. Chem. Res., Synop.* **1988**, 289.
(12) Himeno, S.; Miyashita K.; Saito, A.; Hori, S. *Chem. Lett.* **1990**, 799−802.
(13) Way, D. M. Ph.D. Thesis, Latrobe University, Bundoora, Victoria, Australia, 1996.
(14) Proust, A.; Thouvenot, R.; Robert, F.; Gouzerh, P. *Inorg. Chem.* **1993**, *32*, 5299−5304.
(15) Hori, T.; Himeno, S.; Tamada, O. *J. Chem. Soc., Dalton Trans.* **1996**, 2083−2807.

10.1021/ic991310p CCC: $20.00
Published on Web 12/05/2000

grade), $LiClO_4$ (BDH), H_2SO_4 (BDH, Analar 98%), and acetic acid (BDH, Analar 99.8%). All solvents used were HPLC grade, 99.9% (Mallinckrodt, Biolab Scientific Pty. Ltd.). For electrochemical studies, CH_2Cl_2 was dried over CaH_2 and freshly distilled under a nitrogen atmosphere prior to use and thf was freshly distilled from benzophenone under a nitrogen atmosphere.

$[NHex_4]_2[SMo_{12}O_{40}]$. Solution a: H_2SO_4 (160 μL; 18.8 M) was added to glacial acetic acid (30 mL). Solution b: $HClO_4$ (5.5 mL; 9.2 M) and acetic anhydride (6 mL) were added to glacial acetic acid (35 mL) cooled in an ice bath. The volume was made up to 50 mL. $LiClO_4$ (21.3 g; 170 mmol) and $Na_2MoO_4 \cdot 2H_2O$ (9.7 g; 40 mmol) were dissolved in glacial acetic acid (900 mL) by stirring at ambient temperature. Solution a was added with stirring followed by solution b to give a bright yellow solution, which was diluted to 1 L with acetic acid and stirred at room temperature for 2 h. On addition of $NHex_4Br$ (8.8 g; 20 mmol), a bright yellow salt precipitated, which was filtered off and washed with H_2O and EtOH. The yellow crystals were recrystallized from $MeCN/CH_2Cl_2$ (70/30), washed with EtOH, and dried in a vacuum desiccator. Yield: 6.7 g; 80%.

$[NBu_4]_3[SMo_{12}O_{40}]$. A yellow solution of $[NHex_4]_2[SMo_{12}O_{40}]$ (5 mM) in CH_2Cl_2 (10 mL; $NHex_4ClO_4$, 0.1 M) was reduced at -0.1 V vs Fc^+/Fc until the Faradaic current decayed to zero (about 20 min). Coulometry indicated the transfer of 0.95(5) electrons per molecule. Solid NBu_4Br (4 equiv) was dissolved in the deep green solution, which was refrigerated at 4 °C. Green crystals appeared within 2 days and were isolated by filtration, washed with EtOH and H_2O, and dried under vacuum for 24 h. Yield: 0.75 g; 65%. Negative ion ES-MS (MeCN): 912 ($[SMo_{12}O_{40}]^{2-}$); 608 ($[SMo_{12}O_{40}]^{3-}$).

$[NPr_4]_3[SMo_{12}O_{40}]$. This synthesis differed only in the addition of NPr_4Br (4 equiv) to the green solution after electrolysis. Green crystals precipitated immediately. Yield: (0.95 g; 80%). Found: C, 18.2; H, 3.5; N, 1.7; S, 1.2. $C_{36}H_{84}Mo_{12}O_{40}S$ requires C, 18.1; H, 3.5; N, 1.8; S, 1.3. Negative ion ES-MS (MeCN): 912 ($[SMo_{12}O_{40}]^{2-}$); 608 ($[SMo_{12}O_{40}]^{3-}$).

$[NPr_4]_4[SMo_{12}O_{40}]$. Electrolysis of an equivalent solution at the more negative potential of -0.5 V vs Fc^+/Fc led to a deep blue solution. Coulometry indicated the transfer of 1.95(5) electrons per molecule. Blue crystals were isolated in a same manner to that described above. Yield: 0.95 g; 75%. Found: C, 22.3; H, 4.4; N, 1.9; S, 1.1. $C_{48}H_{112}Mo_{12}O_{40}S$ requires C, 22.4; H, 4.4; N, 2.2; S, 1.2. Negative ion ES-MS (MeCN): 912 ($[SMo_{12}O_{40}]^{2-}$); 608 ($[SMo_{12}O_{40}]^{3-}$).

Electrochemistry. All voltammograms were acquired at 22 °C using a Cypress Systems Model CS-1090 computer-controlled electroanalytical system in the staircase mode. Rotating-disk electrode voltammetry employed a variable-speed rotator (Metrohm 628-10). Solvents used in electrochemical experiments were degassed with dinitrogen that had been presaturated with solvent. The standard three electrode cell electrochemical arrangement was employed. Glassy carbon disk (*d*, 3.0 mm) or rotating-disk (d, 2.8 mm) macrodisk electrodes or microdisk (*d*, 11 μm) were used as working electrodes. The counter electrode was a platinum wire. In dichloromethane studies, the Ag/AgCl reference electrode was a silver wire coated with AgCl in contact with a saturated LiCl solution in CH_2Cl_2, and it was separated from the test solution by a salt bridge containing CH_2Cl_2 ($NHex_4ClO_4$, 0.1 M). For electrochemical experiments in thf, the reference electrode was Ag/Ag^+ which consisted of a silver wire dipped into a MeCN/thf (1/1 v/v) solution of $AgNO_3$ (0.01 M) and NBu_4ClO_4 (0.1 M) separated from the electroactive solution by a porous frit. However, all electrode potentials are quoted relative to the ferrocenium/ferrocence redox couple (Fc^+/Fc).

Digital simulation of cyclic voltammograms was performed with the simulation package DigiSim V 2.1 (Bioanalytical System, West Lafayette, IN)[16] and was run on a 150 MHz Pentium PC. Each simulation required about 5 s.

Bulk electrolysis experiments were carried out using a Bioanalytical System model 100 electrochemical analyzer. The bulk electrolysis cell contained two Pt baskets which served as the working and counter electrodes. The working electrode was arranged symmetrically inside the counter electrode and separated by a glass cylinder with a porous glass frit in the base.[17] The reference electrode (Ag/Ag^+) was positioned as close as possible to the working electrode in order to maximize the uniformity of potential over its surface.

Physical Techniques. Absorption spectra were recorded on a Cary 5 spectrophotometer controlled by a Pentium PC. A rectangular OTTLE cell (path length, 1 mm) with a 3 mL solution reservoir was utilized for spectroelectrochemistry.[18] A Pt gauze (ca 4 cm^2; ca. 75% transmission) working electrode was used to generate reduced species. A silver wire quasi-reference electrode and Pt counter electrode were separated from the electroactive solution by salt bridges located in the upper reservoir of the cell. Electrolysis was performed with a PAR model 273A potentiostat. Potentials were held 100−150 mV more negative than the half-wave potential of the appropriate redox process. All spectra were corrected for background electrolyte absorption.

X-band EPR measurements were made with Varian E-12 and Bruker ESP-380 spectrometers. Unless otherwise stated, EPR spectra were measured at 77 K. Gains in the range 8×10^1 to 2×10^4 and modulation amplitudes between 0.01 and 5.0 G were used. Temperature control was achieved using an ITC4 thermostat (Oxford Instruments Ltd., U.K.). The *g* values were measured via calibration with DPPH.[19] For EPR experiments on electrochemically generated species (coulometric titrations), the reduced solutions were transferred to a degassed quartz EPR tube, which was sealed and frozen in liquid nitrogen.

Variable-temperature magnetic susceptibility measurements (300−4.2 K) were performed on powdered samples at a field strength of 10000 G (1 T) using a Quantum Design M.P.M.S. Squid magnetometer. The calibration of the instrument was checked against $CuSO_4 \cdot 5H_2O$ and a standard palladium sample supplied by the manufacturer. Samples were enclosed in gelatin capsules suspended in the middle of a plastic drinking straw, which was rigidly fixed to the end of the sample rod. The magnetic susceptibilities were corrected for diamagnetic contributions by use of Pascal's tables. For $[NPr_4]_3[SMo_{12}O_{40}]$, $\chi_{dia} = -1031 \times 10^{-6}$ cm^3 mol^{-1}, similar in magnitude to those used recently for salts of one-electron-reduced anions $[PMo_{12}O_{40}]^{4-}$ and $[SiMo_{12}O_{40}]$.[5−20,21] In these studies,[21] it was assumed that deviations from linearity in the χ_m^{-1} versus temperature plots (and corresponding variation of $\chi_m T$ (or μ_{eff}) with *T*) were due to a temperature independent paramagnetic term (TIP) on the cluster. This TIP was large (approximately 1000×10^{-6} cm^3 mol^{-1}) and of a size similar to the χ_{dia} value.[20,21] It was subtracted to leave a linear χ_m^{-1} versus *T* dependence. While a deviation from linearity is observed in the χ_m^{-1} versus *T* plots for $[NPr_4]_3[SMo_{12}O_{40}]$ and $[NPr_4]_4[SMo_{12}O_{40}]$ (see Figure 4), this TIP correction is not included in these plots since the deviation may originate from other sources. Fitting the data for $[NPr_4]_3[SMo_{12}O_{40}]$ to a χ_m versus $1/T$ plot gave a TIP intercept value smaller in size (690×10^{-6} cm^3 mol^{-1}) than those reported in refs 20 and 21 for related systems.

Electrospray mass spectra were recorded on a VG Bio-Q triple quadrupole mass spectrometer using CH_3CN as the mobile phase.

Crystallography. Dark green prismatic crystals of $[NBu_4]_3[SMo_{12}O_{40}]$ were obtained by slow diffusion of diethyl ether into a MeCN solution. Data were measured on a Rigaku AFC6R diffractometer. The structures were solved by direct methods[22] and expanded using Fourier techniques.[23] All non-carbon atoms were refined anisotropically, whereas all carbon atoms were refined isotropically. The

(16) Rudolph, M.; Reddy, D. P.; Feldberg, S. W. *Anal. Chem.* **1994**, *66*, 589A−600A.

(17) (a) Moinet, C.; Peltier, D. *Bull. Soc. Chim. Fr.* **1969**, 690. (b) Fry, A. J. *Synthetic Organic Electrochemistry*; Wiley: New York, 1989; pp 320−325.

(18) Duff, C. M.; Heath, G. A. *Inorg. Chem.* **1991**, *30*, 2528−2535.

(19) Wertz, J. E.; Bolton, J. R. *Electron Spin Resonance. Elementary Theory and Practical Applications*; McGraw-Hill: New York, 1972; p 464.

(20) Le Magueres, P.; Ouahab, L.; Golhen, S.; Grandjean, D.; Pena, O.; Jegaden, J.-C.; Gomez-Garcia, C. J.; Delhaes, P. *Inorg. Chem.* **1994**, *33*, 5180−5187.

(21) Ouahab, L.; Bencharif, M.; Mhanni, A.; Pelloquin, D.; Halet, J.-F.; Pena, O.; Padrou, J.; Grandjean, D.; Garrigou-Lagrange, C.; Amsell, J.; Delhaes, P. *Chem. Mater.* **1992**, *4*, 666−674.

(22) Sheldrick, G. M. *Crystallographic Computing 3*; Oxford University Press: 1985; pp 175−189.

(23) Beurskens, P. T.; Admiraal, G.; Bosmaman, W. P.; de Gelder, R.; Israel, R.; Smits, J. M. M. The DIRDIF-94 program system. Technical Report of the Cystallography Laboratory; University of Nijmegen: The Netherlands, 1994.

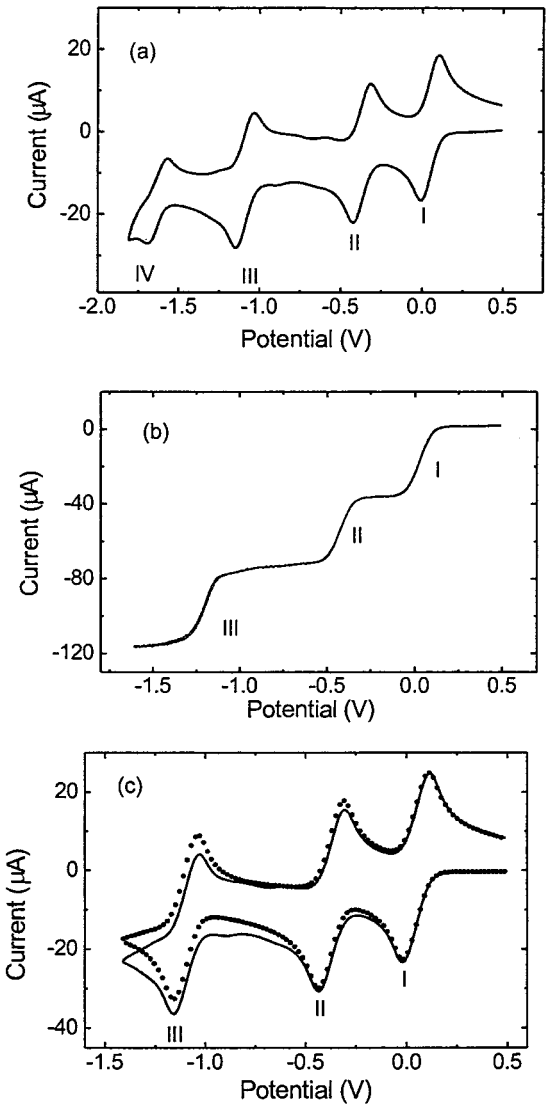

Figure 1. (a) Cyclic and (b) rotated disk electrode voltammograms of $[NHex_4]_2[SMo_{12}O_{40}]$ (2 mM) in CH_2Cl_2 ($NHex_4ClO_4$, 0.1 M): (a) glassy carbon electrode (*d*, 3.0 mm); ν, 0.1 V s^{-1}, (b) glassy carbon electrode (*d*, 2.8 mm); ν, 0.01 V s^{-1}; ω, 500 min^{-1}. (c) Comparison of simulated (···) and experimental (—) cyclic voltammograms for the first three $[NHex_4]_2[SMo_{12}O_{40}]$ reduction processes in CH_2Cl_2. Simulation parameters are as given in text, and experimental conditions are as in Figure 1a.

$[NBu_4]^+$ counterion was refined with restrained bond lengths, and with one of the butyl substituents disordered over two locations. A summary of the crystallographic data is contained in Table 1.

Results and Discussion

Voltammetry. Figure 1a shows a cyclic voltammogram for reduction of α-$[NHex_4]_2[SMo_{12}O_{40}]$ (2 mM) in CH_2Cl_2 ($NHex_4ClO_4$, 0.1 M) over the potential range 0.5 to −1.85 V. Note that for convenience the α isomeric structural designation is normally omitted in subsequent discussion. Four major reduction processes are observed (Table 2). ΔE_p values for processes I and II vary from 0.08 to 0.14 V for scan rates in the range 0.05−1.00 V s^{-1}. These data match those for the known reversible one-electron oxidation of Fc under identical conditions so that departure from ideality can be attributed to the presence of uncompensated resistance. Consequently, the presence of uncompensated resistance means that $E_{1/2}$ values measured as $(E_{pc} + E_{pa})/2$ also are slightly dependent on scan rate. The reversible ($E^r_{1/2}$) values, estimated from slow scan rate data (Table 2) when the uncompensated resistance effect is minimal, are 0.04, −0.37, −1.09, and −1.62 V for processes I−IV, respectively. Exhaustive controlled potential reduction electrolysis of $[SMo_{12}O_{40}]^{2-}$ in CH_2Cl_2 (Hex_4NClO_4, 0.1 M) at −0.1

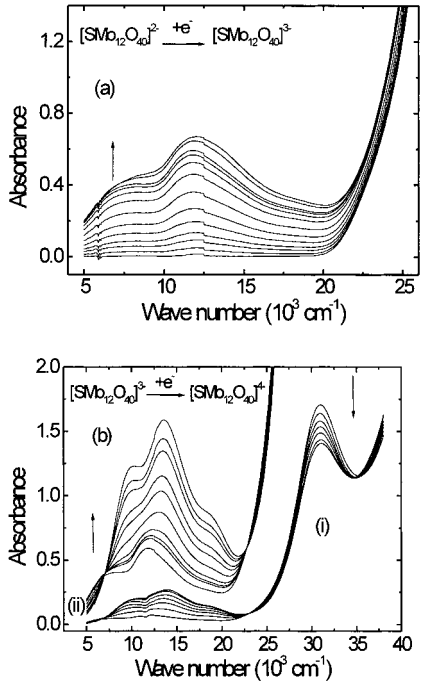

Figure 2. Electronic spectra generated by (a) electrolysis at −0.1 V of $[NHex_4]_2[SMo_{12}O_{40}]$ in CH_2Cl_2 ($NHex_4ClO_4$, 0.1 M), the top trace corresponding to the addition of 1 molar equiv of electrons, and (b) electrolysis at −0.5 V, the top trace of series ii corresponding to the addition of 2 molar equiv of electrons, (i) 5×10^{-3} M and (ii) 4×10^{-3} M.

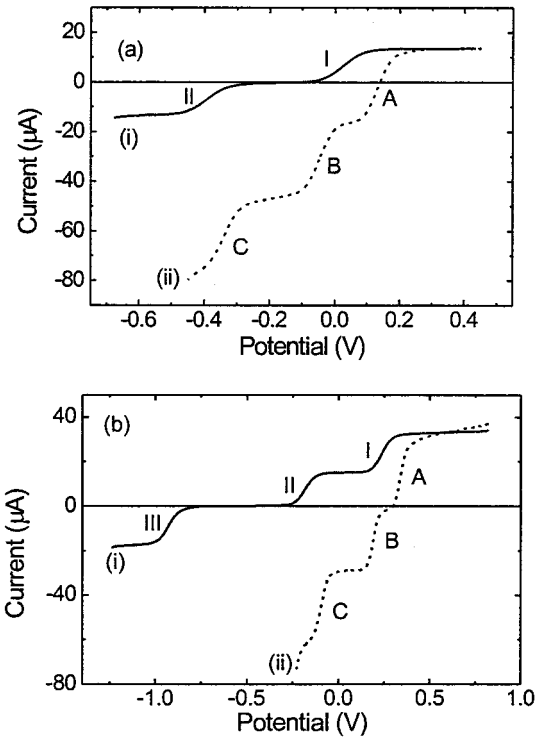

Figure 3. Rotating disk voltammogram of (a) $[NPr_4]_3[SMo_{12}O_{40}]$ in thf/H_2O (98/2; $NHex_4ClO_4$, 0.2 M) and (b) $[NPr_4]_4[SMo_{12}O_{40}]$ in MeCN/H_2O (98/2; $NHex_4ClO_4$, 0.2 M); ν, 0.01 V s^{-1}; ω, 500 min^{-1}. $[HClO_4]$: (i) 0.0 M and (ii) 0.045 M.

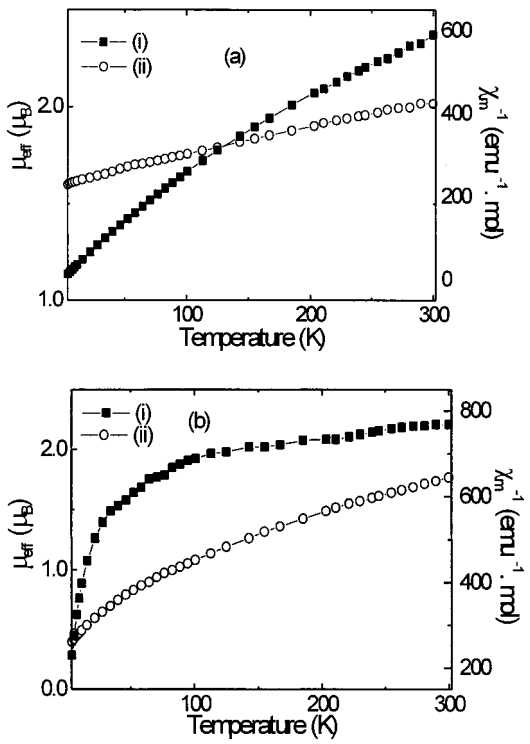

Figure 4. Temperature dependence of magnetic susceptibilities (per mole) and moments of (a) $[NPr_4]_3[SMo_{12}O_{40}]$ and (b) $[NPr_4]_4[SMo_{12}O_{40}]$. (i) χ_m^{-1} and (ii) μ_{eff}. The solid lines merely join the experimental points.

Table 1. Crystallographic Data for $[NBu_4]_3[SMo_{12}O_{40}]$

chem formula	$C_{48}H_{108}Mo_{12}N_3O_{40}S$	fw	2550.72
a, Å	13.840(3)	space group	$P\bar{1}$ (No. 2)
b, Å	15.587(4)	*T*, °C	23 ± 1
c, Å	19.370(3)	λ, (Å)	1.54178
α, deg	94.82(2)	ρ_{calcd}, g cm^{-3}	2.038
β, deg	93.10(1)	μ(Cu Kα), cm^{-1}	152.28
γ, deg	91.05(2)	R^a	0.064
V, Å^3	4156(1)	$R_w{}^b$	0.064
Z	2		

^{a} $R = \sum||F_o| - |F_c||/\sum|F_o|$. ^{b} $R_w = [\sum w(|F_o| - |F_c|)^2/\sum w|F_o|^2]^{1/2}$. $w = [\sigma^2(F_o) + 0.000004|F_o|^2]^{-1}$.

and −0.5 V provided a green and a blue solution, respectively. Coulometry indicated that 0.95(5) and 1.95(5) electrons per molecule, respectively, are transferred. These data confirm that processes I and II each involve one-electron charge transfer steps.

Process III exhibits ΔE_p and i_{pc} parameters similar to those observed for processes I and II and apparently also involves a chemically and electrochemically reversible one-electron transfer. Waves of low current intensity were observed between processes II and IV and were relatively more prominent for concentrations of $[SMo_{12}O_{40}]^{2-}$ <2 mM. They are attributed to reaction of the reduced products of processes II and III with protons from adventitious water in the solvent. These protonation reactions and/or precipitation or adsorption electrode blocking reactions are the apparent cause of the lower peak current of process IV relative to those of I−III (see later). If NBu_4ClO_4 (0.1 M) rather than $NHex_4ClO_4$ (0.1 M) is used as electrolyte, process IV is barely observable, suggesting that precipitation of the three-electron-reduction product $[NBu_4]_5[SMo_{12}O_{40}]$ may occur and give rise to electrode blockage on the voltammetric time scale.

A rotating disk voltammogram for processes I−III is shown in Figure 1b with data listed in Table S1 (Supporting Information). The limiting currents of processes II and III are marginally lower than that of process I, suggesting that surface blocking adsorption or precipitation processes discussed above are influencing the observations at the slow scan rate (0.015 V s^{-1}). The $E_{1/2}$ value for process I was essentially independent of rotation rate ω whereas those for processes II and III shifted to slightly more negative potential as ω increased (Table S1). Plots of potential versus $\log[(i_L - i)/i]$ for each of processes I−III or the so-called "log-plots" at ω, 500 min^{-1} exhibited slopes of 0.080, 0.082, and 0.076 V, respectively, providing further evidence that each process involves a reversible one-electron charge transfer process. The couple Fc^+/Fc exhibits a "log-plots" slope of 0.080 V under the same conditions, again indicating that departures from ideality (slope = 0.058 V) are attributable to uncompensated resistance (ohmic drop).

The voltammetry indicates that, in the absence of adventitious water, $[SMo_{12}O_{40}]^{2-}$ undergoes four consecutive reduction processes I−IV in CH_2Cl_2, each of which involves the reversible transfer of one electron on the voltammetric time scale:

$$\text{I:}\quad [SMo_{12}O_{40}]^{2-} + e^- \rightleftharpoons [SMo_{12}O_{40}]^{3-}\ (E^r_{1/2} = 0.04\ \text{V}) \tag{1}$$

$$\text{II:}\quad [SMo_{12}O_{40}]^{3-} + e^- \rightleftharpoons [SMo_{12}O_{40}]^{4-}\ (E^r_{1/2} = -0.37\ \text{V}) \tag{2}$$

$$\text{III:}\quad [SMo_{12}O_{40}]^{4-} + e^- \rightleftharpoons [SMo_{12}O_{40}]^{5-}\ (E^r_{1/2} = -1.09\ \text{V}) \tag{3}$$

$$\text{IV:}\quad [SMo_{12}O_{40}]^{5-} + e^- \rightleftharpoons [SMo_{12}O_{40}]^{6-}\ (E^r_{1/2} = -1.62\ \text{V}) \tag{4}$$

Digital simulation of cyclic voltammetry for processes I−III by DigiSim V 2.1 employed the following inputs and assumptions:[16,24]

(a) Each species presented in eqs 1−3 was assumed to be unprotonated.

(b) The diffusion coefficient of $[SMo_{12}O_{40}]^{2-}$ was estimated to be 5.0×10^{-6} cm^2 s^{-1} in CH_2Cl_2 at 25 °C[25] and was assumed to be the same for each polyoxometalate species.

(24) Prenzler, P. D.; Boskovic, C.; Bond, A. M.; Wedd, A. G. *Anal. Chem.* **1999**, *71*, 3650−3656.

(25) The diffusion coefficient of $[SMo_{12}O_{40}]^{2-}$ in dichloromethane ($NHex_4ClO_4$, 0.1 M) at 25 °C was determined using (a) the Levich equation for rotated disk voltammetry and (b) microdisk electrode voltammetry under near steady-state conditions. In method a, a plot of i_L versus $\omega^{1/2}$ for the first reduction process gives a straight line with gradient $= 0.62nFAD^{2/3}\upsilon^{-1/6}C = 5.38 \times 10^{-6}$ A s^2 ($R^2 = 0.9987$) or on rearrangement $D = (\text{gradient}\ \upsilon^{-1/6}/0.62nFAC)^{3/2} = 5.0(\pm 0.5) \times 10^{-6}$ cm^2 s^{-1}, where n = number of electrons transferred = 1 electron, F = 96485 C mol^{-1}, A = electrode area = πr^2, in cm^2 (where r = radius of the electrode = 0.14 cm) = 0.07 cm^2, C = concentration of $[SMo_{12}O_{40}]^{2-}$ in the bulk solution = 1.7×10^{-6} mol cm^3, υ = kinematic viscosity of CH_2Cl_2 = 3.3×10^{-3} cm^2 s^{-1}, ω = angular velocity, in s^{-1} = $2\pi f$ (where f is the frequency of electrode rotation, in revolutions per second), D = diffusion coefficient, in cm^2 s^{-1}, i_L = limiting current, in A. (b) With the use of the microdisk electrode technique under near steady-state conditions, the diffusion coefficient of $[SMo_{12}O_{40}]^{2-}$ was calculated using the relationship of $D = i_L/4nFrC = 5.2 \times 10^{-6}$ cm^2 s^{-1} where r = electrode radius = 5.5×10^{-4} cm, i_L = limiting current for the first reduction process = 1.85×10^{-9} A, and other conditions and parameters are as for a.

Table 2. Cyclic Voltammetry Data[a] for $[NHex_4]_2[SMo_{12}O_{40}]$ in CH_2Cl_2[b]

	process I[c]						process II[d]					
scan rate, ν	E_{pc}	E_{pa}	$E_{1/2}$	ΔE_p	$-i_{pc}$	$\lvert i_{pc}/i_{pa}\rvert$	E_{pc}	E_{pa}	$E_{1/2}$	ΔE_p	$-i_{pc}$	$\lvert i_{pc}/i_{pa}\rvert$
0.05	0.004	0.082	0.043	0.078	2.1	0.98	−0.406	−0.330	−0.368	0.076	2.0	0.96
0.10	−0.002	0.084	0.041	0.086	2.6	0.98	−0.414	−0.330	−0.372	0.084	2.6	0.96
0.20	−0.008	0.092	0.042	0.100	3.9	0.99	−0.422	−0.322	−0.372	0.100	3.8	0.97
0.50	−0.022	0.100	0.039	0.122	5.6	0.98	−0.434	−0.322	−0.378	0.112	5.5	0.98
1.00	−0.034	0.108	0.037	0.142	7.7	0.98	−0.450	−0.308	−0.379	0.142	7.5	0.95
	process III[e]						process IV[f]					
scan rate, ν	E_{pc}	E_{pa}	$E_{1/2}$	ΔE_p	$-i_{pc}$	$\lvert i_{pc}/i_{pa}\rvert$	E_{pc}	E_{pa}	$E_{1/2}$	ΔE_p	$-i_{pc}$	$\lvert i_{pc}/i_{pa}\rvert$
0.05	−1.126	−1.048	−1.087	0.078	2.0	0.98	−1.660	−1.572	−1.616	0.088	1.6	0.97
0.10	−1.128	−1.044	−1.086	0.084	2.6	0.96	−1.666	−1.566	−1.616	0.100	2.0	0.96
0.20	−1.138	−1.042	−1.090	0.096	3.6	0.97	−1.682	−1.564	−1.623	0.118	2.7	0.97
0.50	−1.154	−1.036	−1.095	0.118	5.5	0.97	−1.704	−1.560	−1.632	0.144	4.1	0.95
1.00	−1.170	−1.026	−1.098	0.144	7.5	0.95	−1.726	−1.552	−1.639	0.174	5.3	0.95

[a] Units: ν, V s^{-1}; E_{pc}, E_{pa}, ΔE_{p-p}, $E_{1/2}$, V versus Fc^+/Fc; i_{pa}, i_{pc}, μA; i_{pc} values are negative; i_{pc}/i_{pa} is given as the magnitude. [b] 2 mM; $NHex_4ClO_4$, 0.1 M; glassy carbon disk electrode (d = 1.0 mm). [c−f] Switching potentials,V: (*c*) −0.2; (*d*) −0.7; (*e*) −1.6; (*f*) −1.85.

Table 3. Rotating Disk Voltammetry Data for $[NHex_4]_2[SMo_{12}O_{40}]$ in thf/H_2O Containing Different Concentrations of $HClO_4$[a]

	0.1 M			0.15 M			0.2 M		
process	i_L (μA)	$E_{1/2}$ (V)	slope[b] (V)	i_L (μA)	$E_{1/2}$ (V)	slope[b] (V)	i_L (μA)	$E_{1/2}$ (V)	slope[b] (V)
A	−55	0.14	0.064	−45	0.14	0.050	−44	0.15	0.042
B	−50	−0.07	0.063	−32	−0.04	0.045	−38	−0.03	0.040
C	−47	−0.39	0.072	−30	−0.35	0.049	−36	−0.31	0.036

[a] 2 mM; 98/2 thf/H_2O (v/v); $NHex_4ClO_4$, 0.2 M; ν, 0.01 V s^{-1}; ω, 500 min^{-1}. [b] Slope of potential versus $\log[(i_L - i)/i]$ plot.

(c) Processes I−III are assumed to be reversible one-electron-transfer steps with $E^r_{1/2}$ values estimated voltammetrically (eqs 1−4).

(d) Uncompensated resistance (R_u) of 1200 Ω was estimated using the (RC) time constant method available with the BAS100 instrument. This result is consistent with a previous study in CH_2Cl_2.[26]

(e) A double-layer capacitance (C_{dl}) of 2.4×10^{-6} F cm^{-2} was assumed initially and then varied until the theoretical and experimental results in the potential region just prior to the first reduction process agreed satisfactorily.

A comparison of experimental and simulated cyclic voltammograms for processes I−III is shown in Figure 1c. Excellent agreement is observed for process I. Process II shows a good fit for the reduction current, but the simulated oxidation current is slightly larger than the experimental current. As the two waves of low current intensity between processes II and III were not included in the simulation mechanism, the simulation and experimental curves for process III have different baselines. However, the simulated ΔE_p values are in good agreement with the experimental data. The goodness of fit was independent of concentration (1−5 mM) and scan rate, consistent with the assignment of the first three reduction processes I−III to reversible one-electron-transfer steps (eqs 1−3). The complications discussed above precluded simulation of process IV by a mechanism based solely on simple reversible electron transfer and diffusion-controlled theory.

OTTLE experiments were conducted on solutions of $[SMo_{12}O_{40}]^{2-}$ in CH_2Cl_2 (0.1 M $NHex_4ClO_4$). When the potential was held at values more negative than for processes I (−0.1 V) and II (−0.5 V), absorption bands appeared in the range 5000−18000 cm^{-1} (Figure 2; Table S2, Supporting Information). Isobestic points at 7000 and 22700 cm^{-1} are observed for process II, indicating clean formation of the two-electron-reduced $[SMo_{12}O_{40}]^{4-}$ (eq 2). Oxidation of the reduced solutions of $[SMo_{12}O_{40}]^{4-}$ and $[SMo_{12}O_{40}]^{3-}$ quantitatively regenerates $[SMo_{12}O_{40}]^{3-}$ and $[SMo_{12}O_{40}]^{2-}$ in turn, confirming that all three polyoxometalate species are stable in CH_2Cl_2 under the stated conditions. As predicted on the basis of voltammetric data, when more negative reduction potentials were applied, side reactions and electrode blockage occurred which inhibited electrolysis. Consequently, exhaustive bulk electrolysis experiments aimed at generating $[SMo_{12}O_{40}]^{5-}$ and $[SMo_{12}O_{40}]^{6-}$ could not be achieved. The spectroelectrochemical data confirm the chemical reversibility of processes I and II in CH_2Cl_2.

Voltammetry in the Presence of Acid. The possibility of protonation of reduced species influencing voltammetric studies was canvassed above. As CH_2Cl_2 is essentially immiscible with water, experiments were conducted on $[NHex_4]_2[SMo_{12}O_{40}]$ and its reduced forms in thf or MeCN with the deliberate addition of water and aqueous perchloric acid. The $[SMo_{12}O_{40}]^{2-}$ salt, but not the reduced forms, is insoluble in MeCN ($NHex_4ClO_4$, 0.1 M). Solutions of $[NHex_4]_2[SMo_{12}O_{40}]$ (2 mM) in "dry" thf ($NHex_4ClO_4$, 0.2 M) again revealed the presence of three reversible one-electron-reduction processes and a less ideal fourth process. Data were consistent with eqs 1−4, with $E_{1/2}$ values for the first three well-defined processes of −0.03, −0.46, and −1.20 V, respectively. Comparison of data obtained in CH_2Cl_2 reveal the presence of a significant solvent dependence.

Cyclic voltammograms obtained from solutions of $[NHex_4]_2[SMo_{12}O_{40}]$ in acidified thf/H_2O (98/2 v/v; $NHex_4ClO_4$, 0.1−0.2 M; $HClO_4$, 0.2 M) exhibit five chemically reversible reduction processes which are labeled A−E in Figure S1a (Supporting Information) (0.2 M $HClO_4$). Processes A−C are well separated, while D and E overlap. Under the same conditions, steady-state voltammograms also exhibit three well-separated processes A−C (Table 3) and the unresolved processes D and E (Figure S1b). The presence of acid significantly facilitates the reduction of $[SMo_{12}O_{40}]^{2-}$ as evidenced by the large shift in $E_{1/2}$ observed on addition of acid. Additionally, the limiting current per unit concentration in the presence of acid is approximately double that in the absence of acid,

(26) Kadish, K. M.; Ding, J. Q.; Malinski, T. *Anal. Chem.* **1984**, *56*, 1741−1744.

Table 4. Rotating Disk Voltammetry Data for $[NHex_4]_3[SMo_{12}O_{40}]$ (1 mM)[a]

	MeCN [NBu_4ClO_4 (0.1 M)]			thf [$NHex_4ClO_4$ (0.2 M)]		
process	$E_{1/2}$ (V)	i_L (μA)	slope (V)	$E_{1/2}$ (V)	i_L (μA)	slope (V)
I[b]	0.23	23	0.056	−0.03	28	0.062
II[c]	−0.19	−26	0.059	−0.46	−26	0.060
III[c]	−0.79	−25	0.059	−1.20	−26	0.065
IV[c]	−1.37	−24	0.063	*d*	*d*	*d*

[a] Conditions as for Table 3. [b] Oxidation process. [c] Reduction process. [d] Process is not well-defined.

implying that processes A, B, and C are two-electron rather than one-electron processes as found for processes I−IV. The calculated $E_{1/2}$ value of process A in the presence of 0.1−0.2 M $HClO_4$ is independent of technique, but those of processes B and C are apparently shifted to slightly more negative potentials under rotating-disk conditions, as expected in the presence of a small amount of uncompensated resistance. Plots of potential versus $\log[(i_L - i)/i]$ for processes A, B, and C in the presence of 0.2 M [$HClO_4$] provide slopes of 0.042, 0.040, and 0.036 V, respectively, which also is suggestive of reversible two-electron steps. At lower $HClO_4$ concentrations (Table 3), the slopes are more drawn out, as expected for closely spaced one-electron charge-transfer steps or increased uncompensated resistance. The expected value for an electrochemically reversible two-electron process is 0.029 V in the absence of an *iR* drop at 22 °C.[27] The combined limiting current for processes D and E is about twice that for process A, suggesting that the former also each involve overall two-electron-transfer steps. The nature of processes A−E is discussed further below.

Salts of Reduced Anions. The clean electrochemistry observed for processes I and II (eqs 1, 2) for $[NHex_4]_2[SMo_{12}O_{40}]$ in CH_2Cl_2 (Tables 2, S1; Figures 1, 2) allowed electrosynthesis of the one- and two-electron-reduced anions $[SMo_{12}O_{40}]^{3-}$ and $[SMo_{12}O_{40}]^{4-}$, isolated as analytically pure tetraalkylammonium salts (see Experimental Section). Electronic spectra of these salts in MeCN were essentially the same as those obtained by spectroelectrochemistry in CH_2Cl_2 ($NHex_4ClO_4$, 0.1 M; Table S2).

Steady-state voltammograms of $[NPr_4]_3[SMo_{12}O_{40}]$ in "dry" MeCN or thf (NBu_4ClO_4, 0.1−0.2 M) consisted of an oxidation process I and three reduction processes II−IV (Table 4).[28] The zero-current position lies between process I and II (cf, Figures 1b and 3a (upper curve)), as required for the one-electron-reduced species. However, the $E_{1/2}$ values do exhibit substantial solvent dependence (cf. Tables 2 and 3) as found with other polyoxometalate systems. Plots of potential versus $\log[(i_L - i)/i]$ for processes I− IV at ω, 500 min^{-1} were linear of slope 0.056−0.065 V, as required for reversible one-electron-transfer steps, consistent with eqs 1−4.

In the presence of acid ($HClO_4$, 0.045 M), three redox processes labeled A−C are observed over the potential range 0.3 to −0.45 V (Figure 3a). The magnitude of the limiting current for each process A, B, and C in the presence of acid is twice that for I or II obtained in the absence of acid, and the slope of the "log-plot" for processes A and B is 0.032 and 0.030 V, respectively, implying again that each of these processes involves a two-electron charge transfer.[27] The position of zero current bisects process A, suggesting that, in the presence of acid, the one-electron-reduced anion $[SMo_{12}O_{40}]^{3-}$ is protonated initially and then disproportionates to give the oxidized and two-electron-reduced forms:

$$[SMo_{12}O_{40}]^{3-} + H^+ \rightleftharpoons [HSMo_{12}O_{40}]^{2-} \quad (5)$$

$$2[HSMo_{12}O_{40}]^{2-} \rightleftharpoons [SMo_{12}O_{40}]^{2-} + [H_2SMo_{12}O_{40}]^{2-} \quad (6)$$

In the absence of acid, the analogous disproportionation reaction may be written as

$$2[SMo_{12}O_{40}]^{3-} \rightleftharpoons [SMo_{12}O_{40}]^{2-} + [SMo_{12}O_{40}]^{4-} \quad (7)$$

and the disproportionation constant K_{dis} can be estimated via

$$\log K_{dis} = 16.9(E_{II}^\circ - E_I^\circ) \quad (8)$$

where the $E_{1/2}$ values for the one-electron processes I and II are taken as approximations to the formal potentials E_{II}° and E_I°. Thus, $K_{dis} = 10^{-7.4}$ for eq 7 and so $[SMo_{12}O_{40}]^{3-}$ is stable in the absence of acid. In $HClO_4$ (0.045 M), eq 6 goes to completion and process A is plausibly assigned to

$$\text{A:}\quad [SMo_{12}O_{40}]^{2-} + 2H^+ + 2e^- \rightleftharpoons [H_2SMo_{12}O_{40}]^{2-} \quad (9)$$

This behavior in the presence of acid is similar to that observed for the one-electron-reduced Dawson analogue $[S_2Mo_{18}O_{62}]^{5-}$.[29]

Steady-state voltammograms of the two-electron-reduced species $[NPr_4]_4[SMo_{12}O_{40}]$ in "dry" MeCN or thf (NBu_4ClO_4, 0.1 M) are similar to those obtained for $[NPr_4]_3[SMo_{12}O_{40}]$, except that the position of zero current now lies between processes II and III (rather than I and II), as required for a two-electron-reduced species. Processes I−III are also defined clearly in MeCN/H_2O (98/2; NBu_4ClO_4, 0.2 M) (Figure 3b). In the presence of acid ($HClO_4$, 0.045 M), processes I and II are converted to one oxidation process A, and, in addition, two reduction processes B and C are observed (Figure 3b). The magnitudes of the limiting current of processes A−C are twice those of process I or II, and this and all other observations are again consistent with process A being assigned to eq 9. Thus, processes B and C may be assigned to reactions of the kind contained in eqs 10 and 11, although the exact protonation states are uncertain:

$$\text{B:}\ [H_2SMo_{12}O_{40}]^{2-} + 2H^+ + 2e^- \rightleftharpoons [H_4SMo_{12}O_{40}]^{2-} \quad (10)$$

$$\text{C:}\ [H_4SMo_{12}O_{40}]^{2-} + 2H^+ + 2e^- \rightleftharpoons [H_6SMo_{12}O_{40}]^{2-} \quad (11)$$

Two-electron processes D and E (Figure S1) may be assigned analogously. The behavior qualitatively resembles that observed for $[S_2Mo_{18}O_{62}]^{4-}$.[5,6]

EPR and Magnetic Susceptibility Data. Controlled potential electrolysis provided CH_2Cl_2 solutions with variable ratios of the oxidized anion $[SMo_{12}O_{40}]^{2-}$ and its one- and two-electron-reduction products, as assessed by the position of zero current in rotating-disk voltammograms (cf. Figures 1b and 3). EPR spectra of such solutions at 77 K indicated the presence of a single EPR-active species (*g*, 1.947; Figure S2, Supporting Information). Its intensity was a maximum when $[SMo_{12}O_{40}]^{3-}$ was the sole species present and zero when $[SMo_{12}O_{40}]^{4-}$ was the sole species present. Hyperfine structure can be observed

(27) Bard, A. J.; Faulkner, L. R. *Electrochemical Methods. Fundamentals and Applications*; Wiley: New York, 1980; p 290.

(28) While $[Hex_4N]_2[SMo_{12}O_{40}]$ precipitates in MeCN upon the addition of 0.1 M Hex_4NClO_4 electrolyte, the related one- and two-electron-reduced salts $[NPr_4]_x[SMo_{12}O_{40}]$ ($x = 3, 4$) are soluble under the same conditions.

(29) Cooper, J. B.; Way, D. M.; Bond, A. M.; Wedd, A. G. *Inorg. Chem.* **1993**, *32*, 2416−2420.

at 12 K (Figure S2). The spectrum is typical of an isotropic Mo(V) site, consisting of a central ($I = 0$) resonance flanked by six hyperfine lines from those molecules (25 atom %) containing an isotope of nuclear spin $I = {}^5/_2$ (A_{iso}, 5.0 mT). It is apparent that the unpaired electron is thermally trapped on a single Mo atom on the EPR time scale at 12 K.[30]

The magnetic susceptibility of powdered $[NPr_4]_3[SMo_{12}O_{40}]$ was measured as a function of temperature. In the plot of χ_m^{-1} versus temperature shown in Figure 4a, deviation from a linear Curie dependence is noted. The corresponding μ_{eff} value varies from 1.6 μ_B at 5 K to 2.0 μ_B at 300 K. The data are consistent with a one-electron spin system. μ_{eff} values at 300 K reported for related phospho- and silico-Keggin complexes are similar (1.5−1.9 μ_B).[20,21,31] As indicated in the Experimental Section, for data reported for the one-electron-reduced salt $[PMo_{12}O_{40}]^{4-}$, deviations from linearity in the χ_m^{-1} versus temperature plot (and corresponding μ_{eff} or $\chi_m T$ versus T plot) were assumed to be due to temperature independent paramagnetism (TIP) originating from the polyoxometalate cluster.[20,21] After correction for this term, linear χ_m^{-1} versus temperature and corresponding μ_{eff} versus temperature Curie-like plots were observed. If a similar interpretation is adopted for the present compound, then a smaller TIP correction of 690×10^{-6} mol^{-1} cm^3 is required to achieve temperature independence in the μ_{corr} versus temperature plot, with μ_{eff} now being 1.6 μ_B and the Curie constant C equal to 0.318. In general, the singly reduced Keggin ions $[SMo_{12}O_{40}]^{3-}$, $[PMo_{12}O_{40}]^{4-}$, $[PW_{12}O_{40}]^{4-}$, and $[SiW_{12}O_{40}]^{5-}$ all show rather similar $S = {}^1/_2$ magnetic behavior.[10,20,21,31,32]

As discussed above, $[SMo_{12}O_{40}]^{4-}$ produced by electrochemical reduction of $[SMo_{12}O_{40}]^{2-}$ in CH_2Cl_2 (2 mM; $NHex_4ClO_4$, 0.1 M) is EPR silent. Microcrystalline powders of $[NPr_4]_4[SMo_{12}O_{40}]$ exhibited an EPR signal at 77 K (g, 1.93(2)) whose intensity was about 0.2% of that of $[NPr_4]_3[SMo_{12}O_{40}]$ (g, 1.95(2)). However, since the relative intensity and g value varied from sample to sample, the EPR signal may result from impurities or from the presence of small quantities of paramagnetic compounds generated from disproportionation reactions occurring during the crystallization process.

The magnetic properties of $[NPr_4]_4[SMo_{12}O_{40}]$, uncorrected for TIP, are shown in Figure 4b. The μ_{eff} values decrease gradually from at 1.7 μ_B at 300 K to 0.4 μ_B at 4.2 K. The 300 K value is a little less than that for the one-electron paramagnet of $[NPr_4]_3[SMo_{12}O_{40}]$. The sample was very carefully protected from light and air and measured quickly after isolation. The TIP corrected data do not yield a linear χ_m^{-1} versus temperature plot. This behavior is probably indicative of spin−spin coupling possibly combined with electron delocalization at the higher temperatures. A value of ca. 2.45 μ_B would be expected at 300 K for two spins. Since antiferromagnetic coupling and/or delocalization should lead to a zero moment at 4.2 K,[33] the nonzero value might indicate that some oxidation has occurred to the one-electron-reduced species. Further work is required to fully understand the magnetism of the two-electron-reduced compound, but it is apparent that it is not diamagnetic. Presumably, rapid relaxation is responsible for the low intensity of its EPR spectrum. A report of an Evans NMR study of α-$[SiW_{12}O_{40}]^{6-}$ showed it to be diamagnetic in solution.[31] Two recent reviews[10,34] of molecular materials (e.g., TTF^+ and $*Cp_2Fe^+$ salts) of polyoxometalates show that magnetic ions such as $[FeW_{12}O_{40}]^{5-}$ generally display very weak intracluster spin−spin coupling and weak interaction between the cationic and anionic spin centers.

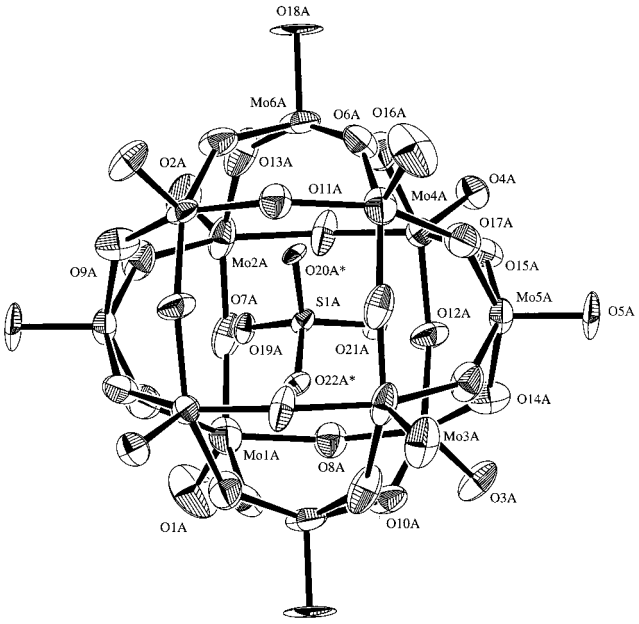

Figure 5. ORTEP representation of the polyoxomolybdate anion in $[NBu_4]_3[SMo_{12}O_{40}]$.

Table 5. Distances (Å) and Angles (deg) of the $SMo_{12}O_{40}$ Moiety in $[NBu_4]_x[SMo_{12}O_{40}]$ ($x = 2, 3$)

parameter[a]	$[SMo_{12}O_{40}]^{2-}$ [b]	$[SMo_{12}O_{40}]^{3-}$ [b]
Mo···Mo	3.581(1)	3.575(2)−3.602(2) [3.59]
S···Mo	3.581(1)	3.575(2)−3.590(2) [3.58]
Mo−O_t	1.649(1)	1.62(2)−1.68(2) [1.65]
Mo−O_b ("short")	1.891(8)	1.79(1)−1.89(1) [1.84]
Mo-O_b ("long")	1.891(8)	1.89(1)−1.95(1) [1.93]
Mo−O(S)	2.52(1)	2.50(2)−2.61(2) [2.55]
S−O	1.480(9)	1.42(2)−1.48(1) [1.46]
O_b−Mo−O_b	86.9(5)	85.1(6)−88.5(6) [86.6]
O_b−Mo−O_t	103.6(4)	101.0(8)−107.9(8) [103.7]
O−S−O	109.5(8)	108(1)−112(1) [109.5]

[a] t, terminal, b, bridging (see Figure 5 for the numbering scheme equivalent to O_b, O_t). [b] Reference 15, the labeling is different in Table 2 of this paper, viz., $O_t = O_d$; $O(S) = O_a$. [c] Mean values in square brackets.

Molecular Structure of $[NBu_4]_3[SMo_{12}O_{40}]$. Three NBu_4^+ cations (one disordered over two locations) were detected per $SMo_{12}O_{40}$ cluster, consistent with the presence of the one-electron-reduced anion $[SMo_{12}O_{40}]^{3-}$ in the dark green crystals. The anion displays the classic α-Keggin structure (Figure 5) as does the oxidized anion in yellow $[NBu_4]_2[SMo_{12}O_{40}]$.[15] The structural parameters for the $1e^-$-reduced and parent clusters are the same, within experimental error (Table 5). By way of comparison,[7] the framework of the ($2e^-$, H^+)-reduced anion $[HPMo_{12}O_{40}]^{4-}$ was slightly expanded over that in the oxidized form $[PMo_{12}O_{40}]^{3-}$. The unit cell of $[NBu_4]_3[SMo_{12}O_{40}]$ contains two independent anions located at inversion centers. The site symmetry −1 is incompatible with the apparent tetrahedral symmetry of the Keggin structure.[32] In fact, the anions are chiral due to displacements of the Mo atoms within the MoO_6 units, leading to alternating "long" and "short" Mo−O−Mo bonds. The disorder imposed is consistent with a model proposed[7] for

(30) Sanchez, C.; Livage, J.; Fournier, M.; Jeannin, Y. *J. Am. Chem. Soc.* **1982**, *104*, 3194−3202.
(31) Kozik, M.; Pastor, N. C.; Hammer, C. F.; Baker, L. C. W. *J. Am. Chem. Soc.* **1988**, *110*, 7697−7710.
(32) Bellitto, C.; Staulo, G.; Bozco, R.; Pecile, C. *Mol. Cryst. Liq. Cryst.* **1993**, *234*, 205.
(33) Borras-Almenar, T. J.; Clemente, J. M.; Coronado, E.; Tsukerblat, B. S. *Chem. Phys.* **1995**, *195*, 1−28.
(34) Ouahab, L. *Chem Mater*. **1997**, *9*, 1909−1926.

salts containing the $[PMo_{12}O_{40}]^{3-}$ and $[HPMo_{12}O_{40}]^{4-}$ anions discussed above. Thus the alternating "long" and "short" Mo−O−Mo bonds are retained but the edge- and corner-shared MoO_6 units are superimposed (cf. Figure 5; Table 5). Other related examples of disorder about the central tetrahedron have been reported.[15,35,36]

Conclusions. The one- and two-electron-reduced species of α-$[SMo_{12}O_{40}]^{2-}$ were generated by reductive electrosynthesis and successfully isolated as tetraalkylammonium salts. Data obtained from voltammetric experiments demonstrated that, in the presence of acid, the one-electron-reduced anion $[SMo_{12}O_{40}]^{3-}$ protonates and disproportionates into $[SMo_{12}O_{40}]^{2-}$ and the ($2e^-$, $2H^+$)-reduced anion $[H_2SMo_{12}O_{40}]^{2-}$. On the other hand, two-electron-reduced $[SMo_{12}O_{40}]^{4-}$ is stabilized by protonation. EPR and magnetic data indicate that $[SMo_{12}O_{40}]^{3-}$ is a simple paramagnet but that $[SMo_{12}O_{40}]^{4-}$ is EPR silent with temperature dependent magnetic moments, probably arising from exchange coupling and delocalization effects.

Acknowledgment. A.G.W., A.M.B., and K.S.M. thank the Australian Research Council for support under Grants A29801726 and A29702937.

Supporting Information Available: Electrochemical figure (Figure S1), EPR figure (Figure S2), and tables of electrochemical data (Table S1) and electronic spectra (Table S2). One X-ray crystallographic file, in CIF format. This material is available free of charge via the Internet at http://pubs.acs.org.

IC991310P

(35) Evans, H. T.; Pope, M. T. *Inorg. Chem.* **1984**, *23*, 501−504.
(36) Gomez-Garcia, C. J.; Gimenez-Saiz, C.; Triki, S.; Coronado, E.; Le Maguerres, P.; Ouahab, L.; Ducasse, L.; Sourisseau, C.; Delhaes, P. *Inorg. Chem.* **1995**, *34*, 4139−4151.